

Examination of Rhythmicity of Extracellularly Recorded Neurons in the Entorhinal Cortex

Jason R. Climer,^{1*} Ronald DiTullio,¹ Ehren L. Newman,¹ Michael E. Hasselmo,¹ and Uri T. Eden²

ABSTRACT: A number of studies have examined the theta-rhythmic modulation of neuronal firing in the hippocampal circuit. For extracellular recordings, this is often done by examining spectral properties of the spike-time autocorrelogram, most significantly, for validating the presence or absence of theta modulation across species. These techniques can show significant rhythmicity for high firing rate, highly rhythmic neurons; however, they are substantially biased by several factors including the peak firing rate of the neuron, the amount of time spent in the neuron's receptive field, and other temporal properties of the rhythmicity such as cycle-skipping. These limitations make it difficult to examine rhythmic modulation in neurons with low firing rates or when an animal has short dwell times within the firing field and difficult to compare rhythmicity under disparate experimental conditions when these factors frequently differ. Here, we describe in detail the challenges that researchers face when using these techniques and apply our findings to recent recordings from bat entorhinal grid cells, suggesting that they may have lacked enough data to examine theta rhythmicity robustly. We describe a more sensitive and statistically rigorous method using maximum likelihood estimation (MLE) of a parametric model of the lags within the autocorrelation window, which helps to alleviate some of the problems of traditional methods and was also unable to detect rhythmicity in bat grid cells. Using large batteries of simulated data, we explored the boundaries for which the MLE technique and the theta index can detect rhythmicity. The MLE technique is less sensitive to many features of the autocorrelogram and provides a framework for statistical testing to detect rhythmicity as well as changes in rhythmicity in individual sessions providing a substantial improvement over previous methods. © 2014 Wiley Periodicals, Inc.

KEY WORDS: theta; grid cell; bat; rat; maximum likelihood estimation

INTRODUCTION

Elucidating the intrinsic and network properties that underlie the firing of neurons is a critical component to how we understand the brain. Researchers performing large-scale, extracellular recordings in animals

commonly attempt to examine these properties via analysis of the timing of action potentials.

In the rodent hippocampal circuit, theta frequency (6–10 Hz) oscillations are a prominent part of the local field potential (Green and Arduini, 1954; Vanderwolf, 1969; Buzsáki et al., 1983; Stewart and Fox, 1991; Buzsáki, 2002). Although the exact mechanism of theta rhythm generation is unclear, neurons in these areas intrinsically generate theta frequency sub-threshold membrane potential oscillations and are resonant to theta frequency inputs (Alonso and Llinas, 1989; Hutcheon and Yarom, 2000; Erchova et al., 2004; Heys et al., 2010; Buzsáki et al., 2012). In the rat, neurons in the hippocampal formation fire theta rhythmically (Fox et al., 1986; Csicsvari et al., 1999; Cacucci et al., 2004; Jeewajee et al., 2008; Boccara et al., 2010; Deshmukh et al., 2010), and the timing of neuronal action potentials relative to the ongoing oscillation carries information about the trajectory of the animal (O'Keefe and Recce, 1993; Burgess et al., 1994; Skaggs et al., 1996; Hafting et al., 2008; Huxter et al., 2008; Climer et al., 2013). Furthermore, entorhinal grid cells, which have periodic receptive fields for the position of a rodent in an environment, lose their spatial tuning when theta is blocked by inhibition of neurons in the medial septum (Brandon et al., 2011; Koenig et al., 2011) in support of models that rely on theta oscillations for the generation of grid cells (O'Keefe and Burgess, 2005; Burgess, 2008; Zilli et al., 2009; Barry et al., 2012). Taken with a wealth of behavioral and single unit coding data, theta rhythmic interactions between neurons have been proposed as an important mechanism underlying function in these circuits (For reviews, see Buzsáki, 2002; Hasselmo, 2005; Zilli, 2012; Colgin, 2013).

In other studies, however, the impact of theta rhythm oscillations on the hippocampal circuit has been disputed. In non-human primates and humans, theta oscillations have been associated with movement planning (Watrous et al., 2011), and spike-field coherence with theta oscillations has been associated with memory function (Tesche and Karhu, 2000); however, the theta rhythm in primates is much less prominent in the local field potential and rhythmicity is less apparent in single units. In rodents, theta rhythm is not required for the function of place cells and

¹ Department of Psychological and Brain Sciences, Center for Memory and Brain, Boston University, Massachusetts; ² Department of Mathematics and Statistics, Boston University, Massachusetts

Additional Supporting Information may be found in the online version of this article.

Grant sponsor: National Institute of Mental Health; Grant number: R01 MH60013; R01 MH61492; and 1F31MH102022-01A1; Grant sponsor: Office of Naval Research MURI award; Grant number: N00014-10-1-0936.

*Correspondence to: Jason R. Climer, Center for Memory and Brain, 2 Cummington Mall, Boston, MA 02215, USA. E-mail: jrclimer@bu.edu
Accepted for publication 14 October 2014.

DOI 10.1002/hipo.22383

Published online 20 October 2014 in Wiley Online Library (wileyonlinelibrary.com).

remapping in new environments (Brandon et al., 2014), and the loss of grid cell tuning associated with medial septal inhibition may be the result of the loss of cholinergic tone (Newman et al., 2014). Recent recordings from bat hippocampus and entorhinal cortex have shown short bouts of theta oscillations and no significant theta in the timing of spiking of neurons outside of these short theta events (Yartsev et al., 2011; Yartsev and Ulanovsky, 2013). In conjunction with other critiques (Remme et al., 2010; Domnisoru et al., 2013; Schmidt-Hieber and Häusser, 2013), these data were interpreted as causal disproof of computational models that rely on theta oscillations and have brought into question the overall role of theta oscillations in cognitive and memory processes.

The canonical way of examining theta rhythmicity of neurons in rodents and bats is the theta index (Jeewajee et al., 2008; Boccara et al., 2010; Deshmukh et al., 2010; Yartsev et al., 2011; Yartsev and Ulanovsky, 2013). However, it has been shown that the theta index is sensitive to lower firing rates, such as those observed in bat grid cells (Barry et al., 2012). There are potential flaws in the analysis of established measures of theta rhythmicity and the effects of differences in firing rate, and thus, an in-depth analysis of rhythmicity measures has been proposed (Yartsev et al., 2012).

Here, using analytical techniques and large batteries of simulated cells, we have examined many features that confound the interpretation of the theta index and would make detection of rhythmicity under many conditions more difficult. In addition, we describe a novel technique for examining theta rhythmicity by estimating the estimated likelihood of spiking as a function of previous spiking history over a range of lags. This technique provides increased power in detecting rhythmicity over the theta index. We have implemented this new technique in MATLAB, and the code is available at https://github.com/jrclimer/mle_rhythmicity.

METHODOLOGY

Grid Cell Recordings

Recordings from rat grid cells have been presented previously (Climer et al., 2013; Newman et al., 2014). Briefly, animals were anesthetized with isoflurane and a Ketamine cocktail (Ketamine 12.92 mg/ml, Acepromazine 0.1 mg/ml, Xylazine 1.31 mg/ml), placed in a stereotaxic holder, and the dorsal skull was cleared of skin and periosteum. Anchor screws were inserted, and one screw was positioned above the cerebellum in contact with the dura, wired to the implant, and used as a recording ground. Recording drives were either single bundle microdrives (Axona Ltd., St. Albans, Hertfordshire, United Kingdom) with four recording tetrodes (4, 12.7-micron nichrome wires twisted together) that could be moved together, or hyperdrives containing 16 tetrodes that could be moved individually. Craniotomies were made ~ 4.5 mm lateral of bregma and near the anterior edge of the transverse sinus.

Microdrives were angled $\sim 12^\circ$ in the anterior direction, and hyperdrives were not angled. Some drives were targeted in line with the ear bars and angled $\sim 12^\circ$ in the posterior direction. The craniotomy was sealed with Kwik-Sil (World Precision Instruments, Shanghai PRC) and the drive was secured with dental acrylic. After at least seven days postoperative recovery, animals were screened for grid cells using criteria from previous studies (Fyhn et al., 2004; Hafting et al., 2005, 2008) as animals foraged in open environments. Rat grid cells shown are 25 grid cells, theta rhythmic by the theta index, from 25 quantiles of the number of lags in the autocorrelogram. Bat grid cell spike times were generously provided by Yartsev et al. (2011).

Examination of Traditional Methods: The Theta Index

The theta index was calculated here as by Yartsev et al., (2011). First, we computed the autocorrelation of the spike train binned by 0.01 s with lags up to ± 0.5 s. Without normalization, this may be interpreted as the counts of spikes that occurred in each 0.01 s bin after a previous spike (Fig. 1a). The mean was then subtracted, and the spectrum was calculated as the square of the magnitude of the fast-Fourier transform of this signal, zero-padded to 2^{16} samples. This spectrum was then smoothed with a 2-Hz rectangular window (Fig. 1b), and the theta index was calculated as the ratio of the mean of the spectrum within 1-Hz of each side of the peak in the 5–11 Hz range to the mean power between 0 and 50 Hz.

The significance of this score has been estimated a number of ways: including an arbitrary cutoff at 5 or by jittering the spike times. Here, we uniformly jittered spike times by ± 10 s and recalculated the theta index. We did this 1,000 times to generate an empirical null distribution and to estimate the significance (P -values) of the theta index (Fig. 1c). Previous studies including Yartsev et al. (2011) have used these high jitters. Such high jitters would not be possible to include in our simulations of the autocorrelogram window and would eliminate all structure including any spatial tuning of the neuron. This may produce a null distribution that is not representative of neurons with the same firing properties as the original cell but are *a priori* not rhythmic. Thus, we also used a smaller jitter: half of the period of the peak frequency from the spectrogram minus 1 Hz. This limits jitters to be between ± 0.05 and ± 0.125 s (range between 0.1 and 0.25 s), and the jitter would be ± 0.083 s for a cell with a peak frequency at 8 Hz (range 0.17 s). This would eliminate any structure at frequencies within 1 Hz and above the peak power in the theta range, removing any theta rhythmicity, while preserving the other properties of the neuron. In 29 of the 50 real bat and rat cells examined, the bootstrapped null distributions were significantly different between these techniques (50 Bonferroni corrected Kolmogorov-Smirnov tests, $P < 0.05/50$). Of these, all of the shuffled distributions had a slightly smaller median (Mean difference -0.57 , standard error 0.06). Thus, a smaller shuffling window made it slightly easier for the theta index to detect rhythmicity by left shifting the null distribution;

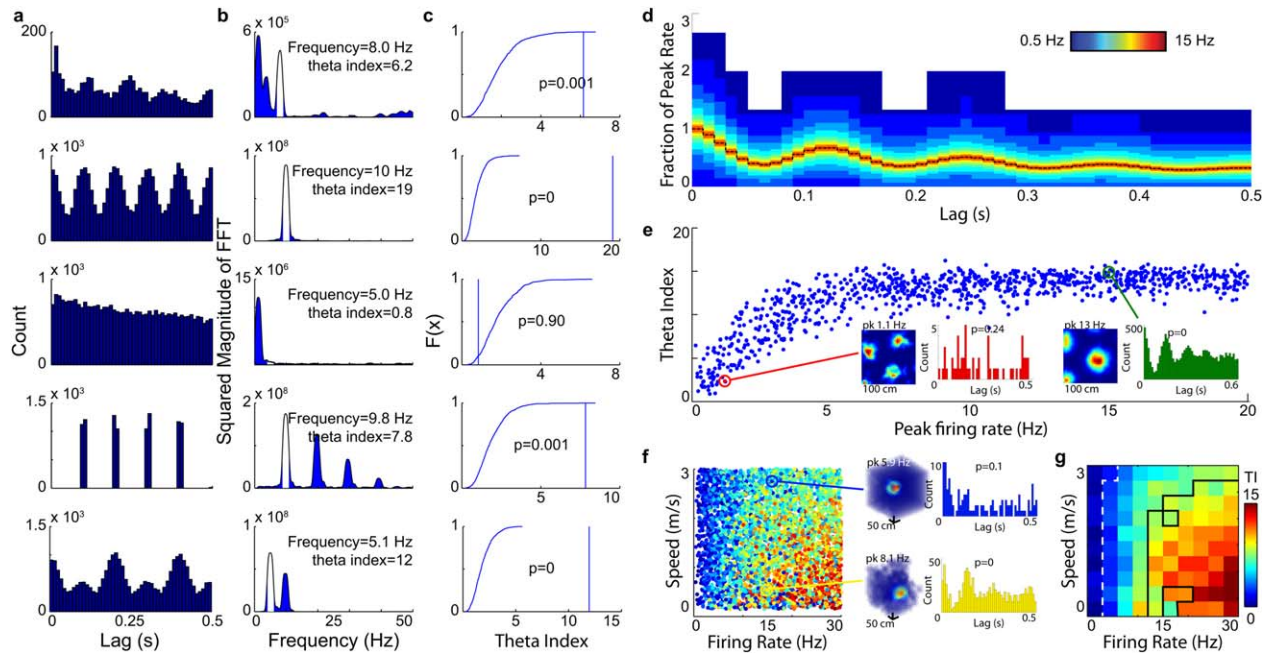


FIGURE 1. Challenges facing traditional methods. a-c.) Theta index analysis for different autocorrelograms generated by a real grid cell (row 1), a perfectly sinusoidally modulated cell (row 2), a cell which ramps off (row 3), a pacemaker (row 4), and a theta-skipping cell (row 5). a.) Spike time autocorrelograms, b.) Smoothed squared magnitude of FFT, c.) Approximation of the null cumulative distribution function (CDF) for the theta index. d.) 95% confidence intervals for the autocorrelogram shape as a fraction of the actual peak rate. Using the same rhythmic baseline rate profile (dashed line), the region that the autocorrelogram will fall with 95% confidence is indicated for a range of peak firing rates. Each shaded area represents a different peak rate, which is modulated at further lags as the dotted line. Peak rates are scaled logarithmically. e.) The theta index decreases at low firing rates.

however, this did not affect the number of significantly rhythmic bat cells.

To illuminate the shortfalls of the theta index, we generated several simulated spike trains as inhomogeneous Poisson processes: one with a rate rising and falling with a 10 Hz sinusoid (Figs. 1a–c row 2); another as a series of linearly decreasing ramps over 1.5 s, separated by 2 s (Figs. 1a–c row 3); a metronome-like cell that randomly omits beats spaced at 0.1 s (Figs. 1a–c row 4); and a theta skipping cell firing on alternate theta cycles using the distribution described by our estimator (Figs. 1a–c row 5). These were all normalized to have the same average firing rate of 10 Hz in the 10 min simulated period.

To generate simulated local field potential theta oscillations, we filtered white noise by the magnitude of the Fourier spectra of entorhinal local field potential recorded from a rat in our laboratory during a foraging task. Similarly, to generate the behavioral data white noise was filtered by the spectra of the speed and angular head direction velocities of the real animal, and the filtered noise was scaled so the power matched the original signal. These signals were integrated to make a path through space, with trajectories being reflected if the animal reached the bound-

ary of the virtual enclosure (1×1 m for 2D, $290 \times 280 \times 270$ cm for 3D). To simulate animals moving at higher velocities, we generated longer patterns of behavior and resampled by interpolation. For example, to simulate an animal moving at twice the original speed we would generate a string of data twice as long and subsample every other position point.

To model the instantaneous firing rate of spatial cells, we used a phasor-model of grid cell precession (Climer et al., 2013) for grid cells and a Gaussian function on the distance from the field center for place cells. The width of the place fields was defined as the diameter of the region in which the firing rate exceeded 95% of the peak rate. Only the magnitudes of the rates were used from these models, so the specific model identity does not affect the neurons' underlying rhythmicity. The resulting signal varied between 0 and 1 as the animal went in and out of the firing field(s). To generate the rhythmicity, this rate was modulated by the square of the positive shifted cosine of the phase of simulated theta LFP. These signals were then scaled so that when the animal was in the field center, they averaged to a peak rate chosen between 0.1 and 20 Hz for the grid cells and 0.1 and 30 Hz for the place cells across a

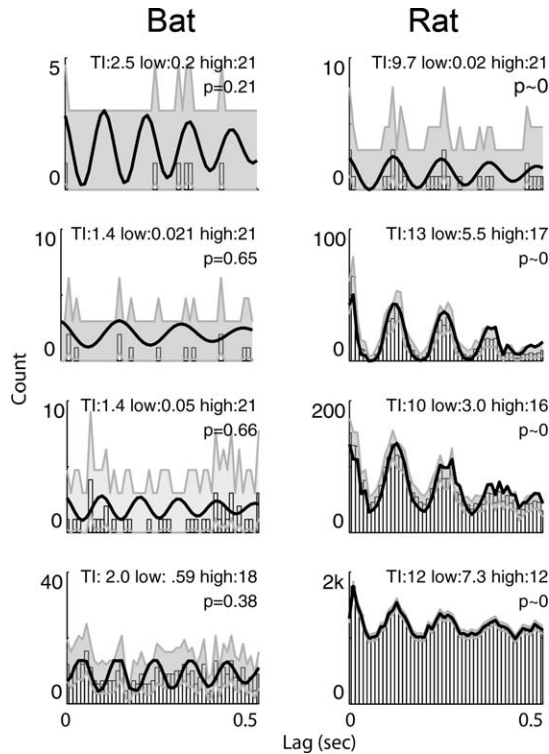


FIGURE 2. Confidence intervals for underlying rate and theta index for bat (left) and rat (right) grid cells. Bars indicate actual counts from the autocorrelograms. For each cell, the gray shaded region indicates the 95% confidence region for the actual underlying rate, given the autocorrelogram count and the number of spikes. The thick black line represents the possible underlying rate with the highest theta index found in this region: these autocorrelograms do not exclude this rhythmic underlying rate, and thus the theta index of this trace is the upper bound of the 95% confidence intervals for the theta index. Actual theta index (TI) and the range of values found in the regions are indicated.

theta cycle. Spike times were then generated using MATLAB's `poissrnd` function and jittering the resulting counts by the LFP sampling frame width. Simulated sessions were 30 min for the 2D grid cells and 40 min for the 3D place cells.

Confidence Intervals on Autocorrelograms and the Theta Index

To generate confidence intervals about the autocorrelogram, we modeled the values in each small time bin of the autocorrelogram as the sum of a series of n poisson processes, where n is the number of spikes. Each lag bin following a spike was modeled as a Poisson process with rate λ_i (in the i^{th} lag bin), which is the true underlying rate estimated by the autocorrelogram. Thus, the total autocorrelogram was modeled as a series of Poisson processes with rate $\lambda_i \times n$. A numerical solution was then found for the range of λ_i , for which the actual count k_i fell within the 95% probability of being produced. This yielded theoretical confidence intervals for the rate profile that underlay a given autocorrelogram, defining bounds within

which the actual underlying rate would fall with confidence. By searching all of the rate profiles in these bounds using MATLAB's `fmincon` function, we can find the most rhythmic and least rhythmic rate profiles that may underlie the firing of the cell with confidence. The theta index of these profiles gives us confidence intervals on the theta index for an individual cell, allowing for us to determine on a cell-by-cell basis if we can exclude high or low values of the theta index.

Maximum Likelihood Estimation (MLE) of the Distribution of Lags

To alleviate challenges arising from the use of the spike-time autocorrelogram, we used MLE to extract parameters from the spike train as follows. First, we calculated the average firing rate of the cell (λ) as the maximum likelihood estimator for a Poisson process: thus, $\hat{\lambda} = \frac{n}{T} \pm C\sqrt{\frac{n}{T^2}}$, where n is the number of spikes, T is the duration of the session, and C is the critical value for the standard normal distribution (for rejection region $P < 0.05$, $C=1.96$).

Then, we took a 0.6 s window following every spike, and we found the lags at which spikes occurred in these windows and marginalized the number of spikes in each of these windows as a Poisson rate. We normalized this by $\hat{\lambda}$ to get an in-window multiplier, M . If k_i is the count of spikes in each window, then $\hat{M} = \frac{k_i T}{n} \pm CT\sqrt{\frac{k_i}{n}}$. For cells with identifiable receptive fields, \hat{M} is typically >1 : a cell's firing rate is higher than its mean when the animal's state is in the cell's receptive field, and the animal is more likely to be in the cell's receptive field if the neuron has just fired.

This left us with a set of m lags at which spikes occurred, x_1, \dots, x_m . We then estimated a parametric model for the marginal distribution of the lag of a spike, given that it occurred within 0.6 s of another spike. This describes many of the features of the autocorrelogram as shown in Figure 3 and Dynamic Figure 1 (available at http://conte.bu.edu/jrclimer/Cli-merEtAl_2014_DynamicFigure1/DynamicFigure1.html). Without skipping, the estimated likelihood (\mathcal{L}) is modeled as:

$$\mathcal{L}(x; \tau, b, c, f, r) = D \left((1-b) \exp\left(-\frac{x}{10^\tau}\right) \left(r \exp\left(-\frac{x}{10^c}\right) F(x) + 1 \right) + b \right) \tag{1}$$

where x is a lag between 0 and 0.6 s, 10^τ is an overall exponential falloff rate [$\log_{10}(\text{sec})$], b is a baseline likelihood (unitless), 10^c is an exponential falloff rate for the magnitude of the rhythmicity ($\log_{10}(\text{sec})$, Vinogradova et al., 1980), f is the frequency of the rhythmic modulation (Hz), r is the rhythmicity factor (unitless), and s is the amount of skipping (unitless). c and τ were made logarithmic, as changes in these values at higher ranges do not appreciably affect the distribution in the examined window. The term D is a normalization factor, such that $\int_0^{0.6} \mathcal{L}(x; \tau, b, c, f, s, r) dx = 1$. With no skipping, $F(x) = \cos(2\pi fx)$.

To add skipping ($s > 0$), we added a second sinusoid, replacing $F(x)$ above with:

$$\frac{(2+2\sqrt{1-s}-s)\cos(2\pi ft)+4s\cos(\pi ft)+2-2\sqrt{1-s}-3s}{4} \quad (2)$$

The above function approaches $\cos(2\pi ft)$ as $s \rightarrow 0^+$. In this function, $1-s$ is the ratio in the heights of the secondary peaks to the primary peaks, that is, when $s=0.5$, the secondary peaks are exactly half of the height of the primary peaks. Additionally, it maintains a constant range of $[-1 \ 1]$. The magnitude of the rhythmic modulation is approximated as the initial magnitude of the rhythmic component: $a=(1-b)r$. a can vary between 0 and 1, with 0 meaning no rhythmicity and 1 meaning maximally rhythmic. To accelerate computation, a discreet approximation was used with a step size of 0.001 s, and integrals were approximated as a left Riemann sum.

The initial guess for the parameters was found using a particle swarm algorithm (Eberhard et al., 2001; Chen, 2014) seeking the maximum log likelihood LL_A using 75 bots searching and initially uniformly randomly distributed across the space $\tau=[-1 \ 1]$, $b=[0 \ 1]$, $c=[-1 \ 1]$, $f=[1 \ 13]$, $s=[0 \ 1]$, $r=[0, 1]$. The peak log likelihood was then converged upon using MATLAB's mle function. MATLAB's mle function also generates confidence intervals (here always 95%) from the estimated Fisher information at the solution arrived upon. To find confidence intervals on the magnitude of the rhythmicity, we then refit the model with all parameters but a fixed, replacing r with $\frac{a}{1-b}$.

This technique artificially treats each lag as an independent observation from a distribution, which artificially inflates the number of degrees of freedom for real cells as the same spike may appear in multiple lag windows. Thus, likelihoods discussed here are only estimated likelihoods (\mathcal{L}). Treating each lag as an independent observation greatly speeds up computation and allows us to analyze rhythmicity without making assumptions about cell types and modeling the rate over slower time scales. Usually a single lag window contains few (<5) spikes, and so this lack of independence does not spread far through the data. In cases where the number of lag windows a single spike appears in is commonly >1 , this may have a number of effects; particularly, confidence intervals estimated from the Fisher information will likely be smaller than if a full distribution were used. Addressing these concerns is a valuable avenue for future research.

Because nonrhythmic and nonskipping represent special cases of this distribution (with $r=0$ and $s=0$ respectively), we then also fit the data as above with r or s fixed to 0, and calculated the log-likelihood of each of these distributions as LL_{0R} and LL_{0S} . To test for significant rhythmicity, we performed a likelihood-ratio (LR) test by calculating the χ^2 statistic as $-2LL_{0R}+2LL_A$, which under the arrhythmic null hypothesis should be distributed on χ^2_{6-2} . Similarly, to test for significant skipping, we can calculate the χ^2 statistic as $-2LL_{0S}+2LL_A$, which under the no-skipping hypothesis should be distributed on χ^2_{6-5} .

To demonstrate this technique, we generated 50,000 sets of lags from 50,000 randomly selected sets of parameters for the distribution described in Eq. (1). The session duration (T , s) was chosen from a \log_{10} scaled uniform distribution between

600 and 3600 s, the peak firing rate (λM) was chosen from a \log_{10} scaled uniform distribution between 0.05 and 40 Hz, and the in window multiplier (M) was chosen from a uniform between 1 and 5. The number of spikes m was then chosen as a Poisson with rate λT , and each of the i^{th} spikes was chosen to have n_i lags following it from a Poisson with rate $\lambda M \times 0.6$. Thus, the total number of marginalized lags (n) followed a Poisson distribution with rate $0.6\lambda^2 TM$, the expected lag count ($E(n)$). A random set of n lags was then generated from the distribution in Eq. (1) and a parameter set chosen randomly from the following uniform distributions: the overall falloff τ ($\log_{10}(sec)$) between -1 and 1 , the baseline b (unitless) between 0 and 1 , the rhythmic falloff c ($\log_{10}(sec)$) between -1 and 1 , the frequency f (Hz) between 0.5 and 15 , the skipping score s (unitless) between 0 and 1 , and the rhythmicity r (unitless) between 0 and 1 . It should be noted that these scores were selected to show a range of values, and that the analysis may return estimators for some of these parameters outside of these bounds.

To test if the overall dataset had changed between 2 separate datasets, we concatenated the sets of lags $x_{1,1} \dots x_{1,m_1}, x_{2,1}, \dots, x_{2,m_2}$, fit, and calculated the log-likelihood of the joint data LL_J . We then calculated the χ^2 -statistic, comparing this to each dataset fit separately: $-2LL_J+2LL_{A1}+2LL_{A2}$, where LL_{A1} , LL_{A2} are the log-likelihoods of independent fits of the first and second data sets under our model respectively. Under the null hypothesis that the data sets came from the same distribution, this is distributed on χ^2_6 . We performed post-hoc LR tests for individual parameter differences by fitting each set of the data with a shared parameter. For example, if comparing the overall falloff τ , the model was $f(x; \tau, b_1, c_1, f_1, s_1, r_1)$ if the lag x comes from the first cell, and $f(x; \tau, b_2, c_2, f_2, s_2, r_2)$ if x comes from the second cell. We then compared this to the separate fits using the χ^2 -statistic ($-2LL_{0\tau}+2LL_{A1}+2LL_{A2}$), where $LL_{0\tau}$ is the log-likelihood of the fit with a shared τ parameter. Under the null hypothesis that the cells share the parameter τ , this is distributed on χ^2_1 . To demonstrate this, we took 25 random parameter sets as described above with $a > 0.75$, $\tau > \log_{10}(0.3)$, $c > \log_{10}(0.3)$, $5 \leq f \leq 11$, and $s \leq 0.25$, a duration of 30 min, an in window multiplier M as above, and the total number of lags in the autocorrelation $\geq 1,000$. We then shifted the 6 parameters of the model by 15 steps and simulated two rhythmicity sets under the resulting parameter sets resulting in 4,500 ($25 \times 15 \times 6 \times 2$) simulations and fit each of these separately. We then performed pair wise comparisons along each axis, resulting in 67,500 comparisons ($25 \times 15 \times 2 \times 6$) and post-hoc tests (Supporting Information Fig. S6).

RESULTS

Challenges Facing Traditional Methods

Canonical examination of theta modulation of firing has depended on the autocorrelation of the binned spike times

(Macadar et al., 1970; Vinogradova et al., 1980; King et al., 1998; Yartsev et al., 2011; Brandon et al., 2013; Yartsev and Ulanovsky, 2013; Ray et al., 2014). An intuitive interpretation of this signal, and the way it is frequently discussed in the literature, is as the counts of spikes that occur in a lag bin following another spike. Figure 1a, row 1 shows a typical example of a spike-time autocorrelogram for a theta modulated grid cell recorded in our lab. Like many rat grid cells, it is moderately theta rhythmic and has a number of features that are useful for demonstrating properties of the theta index. Because the cell is a grid cell, there is an overall falloff of the spike count at further lags due to the increased probability that the animal has left the field. The magnitude of the oscillation also decreases, presumably due to the variability in the frequency of the theta modulation (Vinogradova et al., 1980). Likewise, there is a baseline rate; the troughs of the autocorrelation never go to 0. Finally, the rate of decrease in the size of the peaks is not smooth; the first peak falls off more quickly than the second peak, which falls off less quickly than the third peak. This may suggest a weak cycle-skipping property (Brandon et al., 2013).

The shape of the autocorrelogram is typically analyzed in a scale-free manner, using spectral properties (i.e., theta index) or an alternative fit (see Brandon et al., 2013). However, there is a significant issue with using the shape of the autocorrelogram as an intermediate step; the autocorrelogram becomes extraordinarily variable at relatively low firing rates. If we approximate each bin of the autocorrelogram as a Poisson random count, we can solve analytically for the 95% confidence interval for an autocorrelogram generated by an underlying rate profile. For a given mean rate λ , peak rate $M\lambda$, session duration T , bin width δ , and fraction of the peak rate at the lag Λ , the number of counts is distributed on $Pois(\delta M \Lambda T \lambda^2)$, where $Pois$ is the cumulative Poisson distribution. Thus, as a fraction of the expected peak count, the autocorrelogram will fall between $(Pois^{-1}(\frac{\rho}{2}; \delta M \Lambda T \lambda^2) / \delta M \Lambda T \lambda^2, Pois^{-1}(1 - \frac{\rho}{2}; \delta M \Lambda T \lambda^2) / \delta M \Lambda T \lambda^2)$, and is thus a function of the number of spikes and the relative rate. In Figure 1d, we generated a rhythmic ground truth rate as a fraction of the peak rate, and examined the 95% confidence intervals as a function of peak rate. The average rate was assumed to be 1/3 of the peak rate, and the duration of the sample was 30 min. The color bands show the region that we can say with 95% confidence the approximated autocorrelogram would fall within given the rate profile and the average rate. Note that as the firing rate decreases, there is a sharp increase in the uncertainty of the shape. If the firing rate decreases following a spike, the uncertainty will be greater at larger lags. This has important implications if we are then to do analysis on this shape as any measure of rhythmicity that depends on the spike-time autocorrelogram is negatively biased by the spike rate, the session duration, or by the rate of falloff in the autocorrelogram, even if the cell is known *a priori* to be rhythmic.

In the most common measure of theta modulation, the theta index, the Fourier transform of the autocorrelogram after subtracting the mean is taken, and the peak-squared amplitude in the range between 5 and 11 Hz is chosen as the frequency of the modulation. The theta index is then calculated as the ratio

between the mean squared amplitude in the 2 Hz window centered on this peak, and the mean squared amplitude in a larger window, here between 0 and 50 Hz (as shown in Fig. 1b). The latter window has also been varied (0–125 or 2–125 Hz), and can dramatically alter the results (Barry et al., 2012). The rejection region for the null hypothesis, that the cell is not rhythmic, has either been determined at an arbitrary cutoff (usually $\text{theta index} > 5$) or by generating a null distribution of theta indices after shuffling the data by some window, in this case, ± 10 s (Fig. 1c). There are a number of spectral problems that further bias this score negatively. Because the window has so few samples (usually 100 or 120), there is spectral bleed out, as can be seen in Figures 1a–c, row 2 for a perfectly sinusoidally modulated cell. In the case of a pure 8 Hz sinusoid 100 samples at 100 Hz, this results in 30% of the total power falling in the tails outside of the window. This substantially reduces the theta index as compared with a theoretical theta index with all of the power in the window (18 vs. 25). The spread of spectral power can exacerbate other spectral effects by bleeding power in and out of the theta window, biasing the score towards 1. The slow falloff due to exiting the field adds a large amount of low power structure, which often bleeds into the theta frequency range, as can be seen in Figures 1a–c, row 3 for a cell with a linearly decreasing rate. Non-sinusoidal structure adds large harmonics to the frequency domain, as can be seen in Figures 1a–c, row 4 for a pacemaker cell, whose score is substantially lowered by the higher harmonics. This structure outside of the theta range also bleeds back into the theta window. Finally, other common structures in the rhythmicity, such as theta cycle skipping, disrupt the ability of the theta index to accurately predict the frequency of the modulation and add power outside of the peak range. This can be seen for the theta cycle skipping cell in Figures 1a–c, row 5, where there is more power in the half frequency range of the spectra. This low frequency peak is analyzed by the theta index, despite the obvious theta rhythmic component.

The net result of these problems is that the theta index is substantially biased by many factors, including the peak firing rate and the time spent in the field. We illustrate that by using simulated spatial cells. All of the simulated cells in Figures 1e–g have the same amount of theta rhythmicity: they all fire phase locked to a simulated theta local field potential. In Figure 1e, we simulated 1,000 grid cells with random spacing and orientation that fired locked to the peak of simulated theta with varying peak firing rates, and then we calculated their theta indices. There is a strong correlation ($\rho = 0.71$, $P = 9.6e-155$) between the peak firing rate and the theta index, illustrating the bias of the theta index by firing rate as demonstrated previously. Example cells from the simulated data are shown. Additionally, we simulated 5,000 three-dimensional place cells with random diameter (mean 100 cm) and field center, with varying peak firing rate and varying mean velocity of movement. Figure 1f,g shows these data, with the color of each dot indicating the theta index, and Figure 1g shows the average theta index for the data in 10 speed and rate bins. Sample cells are indicated. Note that at high speeds, the slope of the

autocorrelogram is steeper, and that the highest theta indices are concentrated at high firing rates and low speeds. This can be seen by a significant negative slope of the theta index with increased running speed and decreased firing rate, as well as a significant interaction between running speed and firing rate (GLM speed, firing rate, interaction, $P = 3.9e-73, \sim 0, 1.5e-19$). Subtle features of movement behaviors, such as not stopping or changing direction abruptly, or neuronal properties, such as spike-frequency adaptation, may increase these effects. However, it is clear from these simulations that factors outside of the actual rhythmicity of the neuron bias the theta index.

In real data, if we approximate each small time bin in the autocorrelogram as a Poisson count, we can compute a confidence interval for the underlying “rate profile.” The region of shapes that fall within this range can act as confidence intervals for the theta modulation. If the region excludes highly theta rhythmic signals, it is unlikely that the cell has rhythmicity, rather than we are just unable to detect the rhythmicity. By calculating the theta indices for these profiles, and finding the most and least rhythmic shapes in these regions, we can produce a confidence interval for the theta index for each cell. Figure 2 shows these confidence ranges and the shapes with lowest and highest theta indices which fall within these bounds for 4 bat grid cells from the Ulanovsky laboratory (left) and 4 rat (right) grid cells recorded in our laboratory (For all 25 bat grid cells and 25 rat grid cells, see Supporting Information Figs. S1 and S2). It is worth noting that, due to the wide confidence intervals around the autocorrelation, none of the confidence regions around the bat grid cell autocorrelograms exclude very high theta indices (minimum 17).

The relative width of the confidence intervals around the histogram bars depends on the actual number of spikes counted in that bin. The expected number of observations in a particular bin depends on the product of the trial duration (T), the overall mean firing rate (λ) and the average rate in that bin. The mean firing rates in a bin can be thought of as $\Lambda\lambda$, where Λ is some multiplier of the average firing rate. Usually, within the autocorrelogram window Λ is greater than 1, because the animal is likely to be in a firing field when the cell is firing. Thus, the relative width of the confidence interval depends on $T\Lambda\lambda^2$: the number of observed lags varies quadratically with the firing rate, and linearly with the session duration and the multiplier Λ . Thus, if two cells have the same rhythmic rate multipliers Λ , but one has 1/10 the rate of the other, the session would have to be 100 times as long to have the same reliability in the shape of the autocorrelogram.

Altogether, a more statistically rigorous method of analyzing theta rhythmicity is needed. The theta index cannot be used as a ground truth for how rhythmic cells actually are in the verification of its own efficacy, and thus a systematic exploration of simulated data for which the ground truth rhythmicity is known should be performed. Here, we bypass the use of the spike-time autocorrelogram, and instead estimate the likelihood of the timing of a spike which follows another spike using a parametric model. Using this parametric model, we can generate data for which we know the actual rhythmicity irrespective

of the other factors that may affect the theta index, allowing us to examine how the actual rhythmicity and the other factors affect the theta index.

A Parametric Model of the Distribution of Lags

To reduce the biases of the spike-time autocorrelogram, we generated a new technique using a parametric model of the distribution of lags [Eq. (1), Table 1, Fig. 1a, and Dynamic Fig. 1]. We found all of the lags in 0.6-second windows following each spike, and treated them as independent values from our rhythmicity distribution. Table 1 shows and explains each parameter, and a diagram of the parameters is in Figure 3. To get an intuitive sense of how each parameter affects the shape of the distribution, we encourage the reader to experiment with Dynamic Figure 1, available at <http://bit.ly/1tJurco>. In brief, the distribution models the falloff of firing and the falloff in amplitude of the rhythm as exponentials (Vinogradova et al., 1980), a baseline rate, and the rhythmic modulation as the shifted sum of two cosines, one at half frequency to allow theta cycle skipping. The rhythmicity magnitude, a , is the initial amplitude of the rhythmic component and is what we will use as a metric of rhythmicity. We implemented this in MATLAB, and it is available at https://github.com/jrclimer/mle_rhythmicity.

To compare this technique to the theta index, we simulated 50,000 sets of lags from a range of values under the rhythmicity distribution. We then refit these data to the distribution and then analyzed the data using the theta index. Figure 4a shows the amplitude values, and Figure 4b shows the theta index values. The x-axis has the baseline amplitude of the rhythmicity, and the y-axes show six different ground truth parameters of the distribution. Note that there is very little bias on the estimated amplitude (\hat{a} , Fig. 4a) by the average firing rate \bar{R} , the peak firing rate $\max(R)$, the duration of the session (T), the expected number of lags within the window ($E(n)$), the distribution falloff rate (τ), the baseline rate (b), the falloff rate of the amplitude (c), the frequency (f), or the skipping (s); whereas all of these affect the theta index (Fig. 4b). The maximum (white), median (gray), and minimum (black) values are indicated for the average rate, peak rate as the average rate in the autocorrelogram window, session duration, and lag count for the 25 bat grid cells. Note that, for the theta index, the highest firing rate cell borders the edges where the theta index is always small, and that a change in the session duration has a weak effect on the theta index.

We can quantify these effects using a general linear model (Table 2). To make the slopes comparable, we normalized the theta indices of the simulated cells to their 95th percentile (12.1). Because the relationships between the average and peak firing rate, the session duration, and the expected lag count, we only used the expected lag counts $E(n)$ and the other model parameters τ , b , c , f , s , and a . All factors, with the exception of the baseline rhythmicity, rhythm decay, and skipping score, had a significant effect on the MLE approach (Table 2, $P < 0.05$). The skipping score and rhythm decay do not affect our estimates of rhythmic strength, and the effects of the

TABLE 1.

Parameters of the Parametric Rhythmicity Model [Eq. (1)], Their Range, and Their Description

Parameter	Range	Description
τ	$(-\infty, \infty)$	The log10 of the time constant for the overall decay [log10 (sec)].
c	$(-\infty, \infty)$	The log10 of the time constant for the decay of the rhythmicity amplitude [log10 (sec)].
b	$[0, 1]$	The baseline probability. If 1, the rhythmicity distribution is uniform across the window.
f	$[1, 13]$	The frequency of the rhythmic modulation (Hz).
s	$[0, 1]$	The skipping index. If 0, no skipping, if 1, no secondary peaks.
r	$[0, 1]$	Rhythmic modulation component. If 0, no rhythmic modulation, if 1, maximally rhythmic (given b).
a	$[0, 1]$	$r(1-b)$. The rhythmicity magnitude. The initial relative amplitude of the rhythmic modulation (before normalization).

These values are estimated by and included in the output of our `mle_rhythmicity` function in `stats.phat` or `stats.a`.

baseline b on rhythm strength are encapsulated by the effects of the rhythmicity magnitude a . In contrast, the theta index was significantly affected by all of the factors examined (Table 2, $P < 0.05$). The MLE approach yielded a higher slope on the baseline rhythmicity (0.63 vs. 0.49) and smaller amplitude slopes for interactions with all parameters. These differences were all highly significant (Wald tests, $P \sim 0$).

We can also fit our data with a single exponential decay to a baseline, instead of to an exponential decay with the rhythmic component (Fig. 3). By comparing the log likelihood values from this fit versus the full fit, we can determine if significant evidence exists for the rhythmic model over the arrhythmic model using a likelihood ratio (LR) test. We can do a similar test with s , the skipping score. In Figure 4c, we show the results of LR-tests for the presence of rhythmicity, and in Figure 4d, we show the results of the significance of the shuffled theta index. It is important to note that the specific method of determining the significance of the theta index may change the specific percentage values, and because we only simulated within the autocorrelogram window, we used a smaller shuffling window ($\pm 1/(\text{peak frequency} - 1)$ s). This may cause the detection rates to be higher here than with larger shuffling windows (e.g., 10 s, see methods). All of these simulations have some rhythmicity *a priori*, although the magnitude of this rhythmicity ranges from nearly none to an initial rhythmic amplitude spanning the autocorrelogram. Note that, unlike the estimation of the amplitude, detection of rhythmicity by the MLE approach is also always affected by the expected number

of observed lags in both the theta index and our method. Again, the peak, median and minimum average rates, peak rates, session duration, and spike counts for bat cells are indicated.

Some restrictions apply to the MLE approach. For very small lag counts, it over-fits small numbers of lags with high rhythmicity: it is relatively easy to pick a frequency of oscillation for which a handful of spikes fall at the peaks of the oscillation. These values have very wide confidence intervals about the estimation for a . Thus, we recommend that the value of a should only be used if at least 100 lags are present in the autocorrelogram window (At >95 lags, estimated a is less than 1 standard deviation from the expected average for $a < 0.5$). In contrast the theta index is always biased by the number of lags and at the same number of lags, the theta index is always low in the region where the MLE approach is affected (At <95 lags, mean theta index is 2.3 ± 0.04 standard error for $a > 0.5$). The median number of lags for the rat grid cells examined is 2,042. Because of the artificial independence assumption for lags, the confidence intervals on our lag distributions are likely smaller than if the full distribution were described and a bias may be induced in some of the parameters. Additionally, the frequency of the underlying rhythmicity affects analysis by both techniques. The highest theta indices are restricted to a narrow frequency range around 8 Hz, and detection of rhythmicity by the theta index is highly reduced outside of the 5–11 Hz range. In contrast, the frequency of the underlying rhythmicity has a smaller effect on the amplitude estimation and significance as determined by the MLE approach, but detection breaks down at very low frequencies (<1 Hz). Other factors have effects on the approaches as well. These effects are neither necessarily independent nor additive, and thus, any single subplot in Figure 4 cannot be thought to be completely predictive of detection ability in a dataset.

To examine the effects of parameters on rhythmicity detection, we can generate a logistic generalized linear model (Table

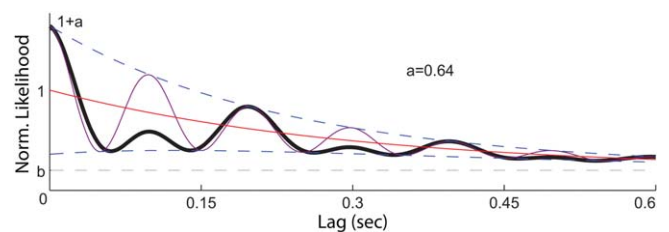


FIGURE 3. Diagram of the parametric rhythmicity distribution, described in Eq. (1). The gray dashed line shows the baseline (b), and the red line shows the falloff, an exponential with rate determined by 10^c . The blue dotted lines show the envelope of the rhythmic modulation, which starts at $a = (1 - b)r$, and falls off with the product of the overall falloff and an exponential with rate 10^τ . In $s = 0$, the rhythm fills this space (solid purple line). If $s > 0$, then a second sinusoid at half frequency is added (thick black line). The amplitude of the oscillations and midline are shifted so the oscillation always fills the space between the decays (dotted blue lines) and so if τ and c are large, the secondary peaks are $(1 - s)$ the height of the primary peaks. [Color figure can be viewed in the online issue, which is available at wileyonlinelibrary.com.]

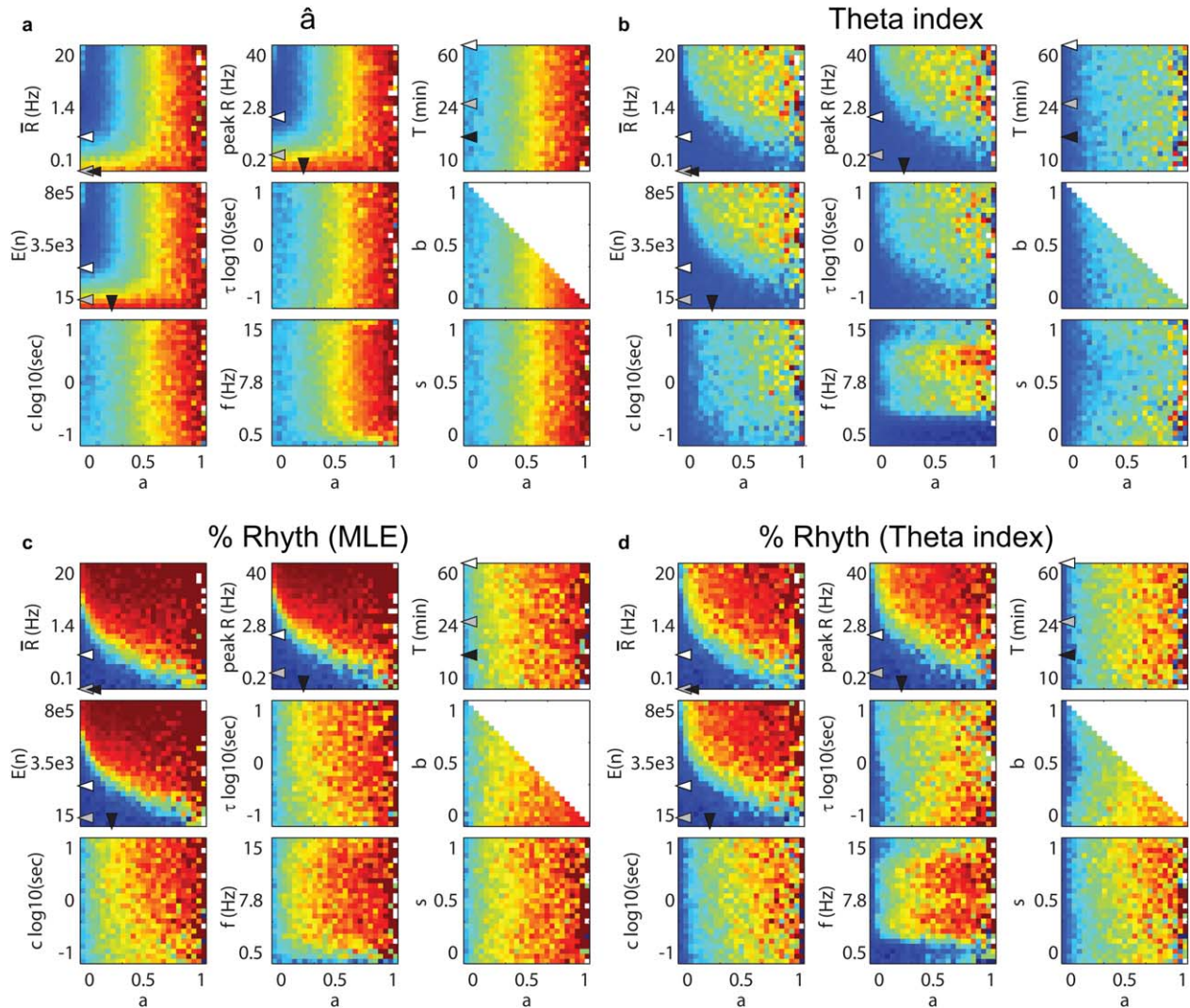


FIGURE 4. Examination of the MLE approach versus the theta index for a simulated dataset a.) Mean of the maximum likelihood estimator for amplitude of rhythmicity (\hat{a}) for 50,000 cells as a function of the ground truth amplitude (x-axis, a), versus several parameters (y-axis): the average spike rate [R (Hz), log axis], the peak spike rate [max (R ; Hz), log axis], the session duration [T (min), log axis], the expected number of spikes in the window [$E(n)$, log axis], the overall falloff rate (τ), the baseline (b), the frequency (f), the rhythmicity fall off (c), and the amount of skip-

ping (s). Maximum is 1. Arrows indicate the highest (white), median (gray), and minimum (black) values of bat grid cells. b.) As a, but for the theta index. Maximum is the 95th percentile of scores, or 12. c.) As a–b, but showing the rate of detection of significant rhythmicity using the MLE method. Maximum is 100%. d.) As a–c, but showing the rate of detection of significant rhythmicity using the theta index. Maximum is 100%. [Color figure can be viewed in the online issue, which is available at wileyonlinelibrary.com.]

3). Higher β values from the logistic fit indicate a sharper transition in the probability of detection along that parameter; thus, higher β values reflect an effect of a parameter over less of the space. The MLE approach yields significantly higher β values for many of the parameters (Table 3, $P < 0.05$) and detected rhythmicity in significantly more of the sessions (54% vs. 41%, binomial test, $P = 0$). Thus, the MLE approach is significantly more sensitive (more simulated cells were significant) to rhythmicity than the theta index under the examined conditions.

We ran our technique on the same cells shown in Figure 2 (Fig. 5, see also Supporting Information Figs. S4 and S5). Again, we were unable to detect significant rhythmicity in any of the bat

grid cells; although, we were able to detect rhythmicity in all of the rat grid cells examined. For many of the bat grid cells, the confidence bounds surrounding our estimate spanned the entire range, indicating that more lags would be required to make an accurate determination about the magnitude of rhythmic modulation of the cells. The best fits of the bat cells contained slow frequency components, but this may not have been significant due to the fast falloff relative to the rhythmic component or the short window size. Although more of the bat grid cells fall within the detection region for the MLE approach, most of the cells do not (Fig. 4c). To demonstrate this, we simulated autocorrelograms with the session duration, mean and peak firing rates

TABLE 2.

General Linear Model Fit of the Fit Amplitude (\hat{a}) or the Theta Index (TI)

Parameter	$\beta_{\hat{a}}$	$P_{\hat{a}}$	$R_{\hat{a}}^2$	β_{TI}	P_{TI}	R_{TI}^2	$\Delta \beta $	% Difference (TI – MLE)
Constant β_0	0.23	~ 0	–	$-5.1e-3$	0.33	–	-0.22	-191%
Expected lag count $E(n)$	$-1.8e-7$	$6.8e-153$	$9.9e-3$	$3.3e-7$	~ 0	0.032	$1.5e-7$	58.7%
Overall decay τ	-0.018	$2.3e-22$	$1.4e-3$	0.12	~ 0	0.054	0.10	147%
Baseline b	$4.4e-3$	0.38	0.099	0.082	$1.6e-51$	0.026	0.077	179%
Rhythm decay c	$-2.1e-4$	0.91	$9.7e-8$	0.049	$3.3e-128$	$9.0e-3$	0.049	198%
Rhythm freq. f	$3.5e-3$	$6.5e-40$	$2.4e-3$	0.016	~ 0	0.047	0.012	128%
Skipping s	$1.2e-4$	0.97	$1.1e-5$	-0.029	$6.0e-13$	$6.7e-4$	0.029	198%
Ground truth amplitude a	0.63	~ 0	0.23	0.49	~ 0	0.097	-0.13	-23.5%

The slope for the fit amplitude ($\beta_{\hat{a}}$) and the theta index (β_{TI}) versus each interaction and their significance ($P_{\hat{a}}$ and P_{TI} , respectively) are indicated. $R_{\hat{a}}^2$ and R_{TI}^2 show the fraction of the variance explained by each interaction alone on the fit amplitude and theta index, respectively. The difference in the slope magnitude ($\Delta|\beta|$) and the percentage difference ($100 \frac{2(|\beta_{TI}| - |\beta_{\hat{a}}|)}{|\beta_{TI}| + |\beta_{\hat{a}}|}$) are also indicated. These differences are all highly significant (Wald tests, $P \sim 0$).

matching the 25 bat grid cells (Supporting Information Fig. S3). For each bat cell, 50 autocorrelograms were generated in 6 bins of the ground truth amplitude and the distributions of values above. We then used the theta index and MLE approaches to detect rhythmicity in these simulations. None of the cells reached 95% detection rates, even when the ground truth amplitude was near 1. In less than half (10/25 for MLE, 9/10 for theta index) of the cells, detection rates ever exceeded 50%. Although many factors may affect rhythmicity detection as discussed above, it is likely that rhythmicity similar to the rhythmicity of rat grid cells would go undetected in most of the bat cells (Mean amplitude for rat grid cells: 0.60). The highest firing rate handful of neurons may imply that rhythmicity is weaker, different (i.e. in a very low frequency), or nonexistent in the bat entorhinal cortex; however, we do not have sufficient evidence to distinguish these from difficulty in detection.

A notable advantage of the MLE approach is that each lag is a separate observation. In contrast to other techniques which “collapse” each spike into a single observation per session (i.e., the theta index of a cell in a particular session), this allows for statistical comparison of a single cell across two sessions using LR-tests comparing the separate fits to those with overlapping parameter estimates. To demonstrate this capability, we took 25 parameter sets that would be favorable for such analysis, shifted each of the parameters over a range in 15 steps, and pairwise compared the results within the same initial parameter tests to show the sensitivity of these tests. The results of this analysis are shown in Supporting Information Figure S6. Under these conditions, the detection of parameter differences is highly sensitive and specific.

DISCUSSION

Recent recordings from the bat entorhinal cortex (Yartsev et al., 2011) and hippocampus (Yartsev and Ulanovsky, 2013)

have shown rate maps which bear spatial structure through grid firing in entorhinal cortex and place fields in hippocampus, but researchers were unable to identify a robust theta rhythmic component in the local field potential or spiking of these neurons. Such findings have been presented as causal disproof of models of spatial firing that rely on theta rhythmic processes. On the other hand, evidence suggesting that theta frequency dynamics carry spatial information (O’Keefe and Recce, 1993; Burgess et al., 1994; Skaggs et al., 1996; Hafting et al., 2008; Huxter et al., 2008; Climer et al., 2013), that theta phase regulates information flow in the hippocampus (Colgin et al., 2009; Belluscio et al., 2012; Newman et al., 2013), and that theta phase regulates hippocampal plasticity (Hölscher et al., 1997; Hyman et al., 2003) support the distinct hypotheses in which theta rhythmic processes are critical to episodic memory and spatial navigation. Some of these processes may be supported by non-rhythmic or very slow oscillations, as in coordination during up and down states during sleep (e.g. Hahn et al., 2012); however, proposed mechanisms of synchronous communication through neural rhythms (Gutkin et al., 2005; Ermentrout et al., 2008; Uhlhaas et al., 2009; Zhou et al., 2013) and theta generation (Dragoi et al., 1999; Buzsáki, 2002; Buzsáki et al., 2012; Spaak et al., 2012) are distinct from those underlying the periodic depolarizations of neurons in these states (Sanchez-Vives and McCormick, 2000; Bazhenov et al., 2002; Sanchez-vives et al., 2010; Mattia and Sanchez-Vives, 2012), and the experimental distinction between the two in the hippocampal circuit is a valuable experimental pursuit.

It has been proposed that the traditional method of measuring theta rhythmicity, the theta index, may be substantially biased by factors such as firing rate (Barry et al., 2012). To this end, we have completed an in-depth analysis of how properties of simulated spatial cells including firing rate (Figs. 1d,e) and movement speed (Fig. 1f) affect the theta index. To combat these issues, we have developed a novel technique using MLE of the distribution of lags to examine rhythmicity, which is more sensitive and robust than the theta index (Figs. 3–5). To verify this technique and to compare with the theta index, we

TABLE 3.

Logistic Fit of the Probability of Detecting Rhythmicity

Parameter	β_{MLE}	P_{MLE}	β_{TI}	P_{TI}	P_{Δ}
Constant β_0	-1.7	3.1e-249	-2.0	~ 0	1.7e-11
Expected lag count $E(n)$	4.9e-5	~ 0	3.8e-6	~ 0	~ 0
Overall decay τ	0.24	9.8e-37	0.12	7.2e-13	5.5e-11
Baseline b	-0.48	3.6e-21	-0.35	4.3e-14	6.5e-3
Rhythm decay c	0.30	8.6e-55	0.22	7.2e-38	2.0e-5
Rhythm freq. f	0.064	7.4e-124	0.082	5.4e-250	8.3e-13
Skipping s	5.1e-3	0.90	0.33	4.7e-21	~ 0
Ground truth amplitude a	3.3	~ 0	3.1	~ 0	6.4e-4

β_{MLE} shows the β values for the fits for the MLE approach, P_{MLE} indicated the significance of each β value for the MLE fit, β_{TI} shows the β values for the theta index, and P_{Δ} shows the significance of the Wald test for the difference between the β s.

simulated and analyzed 50,000 sets of lags with a wide range of properties. Estimated rhythmicity amplitude from the MLE approach was much less biased than the theta index by nearly all features (Fig. 3, Table 2), and rhythmicity detection was more sensitive (Figs. 4c,d, Table 3).

Although providing a notable improvement over the theta index, the advantages of the MLE approach are not without caveats. At very low (<100) lag counts, the method overestimates the amplitude of rhythmicity. As implemented here, it assumes lags are independent, which we know they are not in real data where spikes may appear in multiple lag windows. This increases the degrees of freedom for the dataset analyzed relative to the actual degrees of freedom in the data, which may affect our measures and inappropriately narrow confidence intervals estimated from the Fisher information at high firing rates. Ameliorating these issues would provide notable improvements to rhythmicity measuring techniques.

Since the theta index is a measure on the spike-time autocorrelogram, we have examined the autocorrelograms of the bat grid cells in terms of the expected variability given the actual autocorrelogram counts and numbers of spikes, and we argue that the bat grid cells' autocorrelograms do not contain enough spikes to conclusively determine that they are not rhythmic by the theta index or the MLE approach (Figs. 2, 4, and 5, Supporting Information Figs. S1, S3, and S4). Because of their low firing rates, a low amount of data exists in the lag window. However, we do not rule out the possibility that no theta rhythmic phenomena exist in the bat hippocampal circuit. Indeed, it is unlikely that cells firing with the low rates seen in the crawling bat could reliably carry temporal information as seen in the rodent. Whether the bat hippocampal circuit uses timed activity and processes in memory and spatial navigation as seen in other mammals (O'Keefe and Recce, 1993; Tesche and Karhu, 2000; Hyman et al., 2003; Hafting et al., 2008; Davidson et al., 2009; Addante et al., 2011; Watrous et al., 2011; Climer et al., 2013) remains an open question.

Hippocampus

The higher peak firing rates and larger field size seen in place cells in the flying bat (mean peak firing rate ~ 9 Hz, see Yartsev and Ulanovsky, 2013 Fig. 4e) would be much better suited for such analysis (Fig. 4). These cells also do not show theta rhythmicity via the theta index. However, firing rate is not the only property of cells that biases the theta index and alters detection rates. The autocorrelograms of bat place cells have a very fast falloff (see Yartsev and Ulanovsky, 2013 Fig. 4, Supporting Information S18 and S21), and thus traditional methods may be ill suited for examination of rhythmicity in these cells (Fig. 4b, τ). This falloff may be caused by the fast movement speed of the animals (Fig. 1f), although this may also be caused by intrinsic firing properties that repress long periods of firing. *In vitro* recordings of bat stellate cells have revealed resonance frequencies at much lower frequencies (~ 1.67 Hz) than the canonical theta range in rats (~ 8 Hz; Heys et al., 2013). Rhythmicity at these frequencies would be impossible to detect with the theta index (Fig. 4c) and would require very long, sustained periods of activity in order to be detected by any technique. It would be highly beneficial to examine the bat place cell dataset with the MLE approach or alternate techniques, using a wider examination window to detect whether these slower rhythms exist. Given their

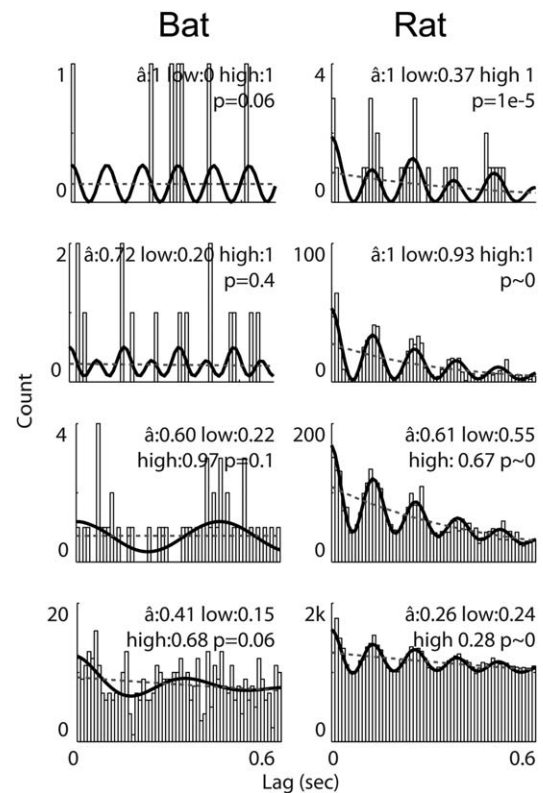


FIGURE 5. MLE method results for bat (left) and rat (right) grid cells analyzed in Figure 2. The dark black line shows the approximated histogram from the best fit, the gray dotted line shows the best fit without rhythmicity. Amplitude of the oscillation (\hat{a}) and 95% confidence intervals are indicated. P -values are the results of the LR test for the full fit (black line) over the non-rhythmic fit (dashed line).

consistently high firing rates and strong rhythmicity in the rodent, GABAergic interneurons may also provide a better platform for examining if a theta-like process exists in the bat brain.

In specific reference to models of grid cells, although several challenges face variants of theta-dependent models (e.g., oscillatory interference, see Remme et al., 2010; Zilli, 2012; Domnisoru et al., 2013 for discussion) they are not mutually-exclusive of other models, and computational models that use multiple mechanisms for generating grid cell firing can capture many features of grid cell activity (Zilli, 2012; Schmidt-Hieber and Häusser, 2013; Bush and Burgess, 2014). It is possible that certain behaviors and mechanisms underlying grid cell behaviors, particularly those of temporal coding, are not present or have become vestigial in the hippocampal circuit of other mammals.

Other aspects, which are not examined here, of rhythmicity may make it difficult to observe. Because we know that these processes are history dependent, the variance of the true distribution may be higher than expected for a consistent Poisson in each bin (e.g., Fenton and Muller, 1998). This would decrease our confidence of the underlying rates, and thus decrease our confidence in the strength of the rhythmicity, widening the confidence intervals about the autocorrelogram and making it more difficult to examine rhythmicity via the theta index. Unexplained variance in the counts may be explained by further conditionalization of the distribution of lags by other features that impact spiking and rhythmicity, such as the frequency of the ongoing LFP oscillation. Theta frequency is variable. In rodents, it is heavily modulated by speed (Richard et al., 2013; Long et al., 2014) and behavior (Belchior et al., 2014), and in both rodents and humans it is modulated by novelty (Sambeth et al., 2009; Park et al., 2014). MLE can provide a framework for examining if significant variance can be explained by this conditionalization of the underlying frequency on any number of factors.

When performing extracellular recordings *in vivo*, it is necessary to estimate intrinsic properties of neurons based on much noisier and poorly understood extracellular potentials. In the face of this challenge, researchers have typically extrapolated analysis on the discrete events of action potentials to determine properties of individual neurons and the larger network. As in any statistical analysis, these tools use data replete with noise to estimate an underlying property of the neuron. As a result, we often try to use tools that average hundreds or thousands of spikes, such as rate maps, with the assumption that with enough data such measures can approximate underlying continuous features of cells. All of these assumptions can break down at lower spike numbers. MLE of parametric distributions provides a powerful alternative approach. By treating each spike as an observation from a distribution, we can find the distribution that was most likely to have generated our data. Because these techniques treat each spike as an observation, we can examine if significant changes exist in the rhythmicity of a single cell in two experimental conditions using LR tests (Supporting Information Fig. S6). When any statistical analysis fails to reject a null hypothesis, particularly with a small number of observa-

tions, researchers should be cautious in how they interpret their null result: the absence of evidence is not necessarily evidence of absence.

Acknowledgments

The authors would like to thank Nachum Ulanovsky for graciously sharing the bat grid cell data with us for further analysis. They would also like to thank G. William Chapman IV, Siobhan T. B. Climer, Jonathan J. Cannon, James R. Hinman, Nancy J. Kopell, and Caitlin K. Monaghan and members of the Cognitive Rhythms Collaborative (NSF-DMS-1042134) for advice and comments.

REFERENCES

- Addante RJ, Watrous AJ, Yonelinas AP, Ekstrom AD, Ranganath C. 2011. Prestimulus theta activity predicts correct source memory retrieval. *Proc Natl Acad Sci USA* 108:10702–10707.
- Alonso A, Llinas RR. 1989. Subthreshold Na-dependent theta-like rhythmicity in stellate cells of entorhinal cortex layer II. *Nature* 342:175–177.
- Barry C, Bush D, O'Keefe J, Burgess N. 2012. Models of grid cells and theta oscillations. *Nature* 488:E1–2.
- Bazhenov M, Timofeev I, Steriade M, Sejnowski TJ. 2002. Model of thalamocortical slow-wave sleep oscillations and transitions to activated States. *J Neurosci* 22:8691–8704.
- Belchior H, Lopes-Dos-Santos V, Tort ABL, Ribeiro S. 2014. Increase in hippocampal theta oscillations during spatial decision making. *Hippocampus* 00:1–10.
- Belluscio MA, Mizuseki K, Schmidt R, Kempter R, Buzsáki G. 2012. Cross-frequency phase-phase coupling between θ and γ oscillations in the hippocampus. *J Neurosci* 32:423–435.
- Boccarda CN, Sargolini F, Thoresen VH, Solstad T, Witter MP, Moser EI, Moser MB. 2010. Grid cells in pre- and parasubiculum. *Nat Neurosci* 13:987–994.
- Brandon MP, Bogaard AR, Libby CP, Connerney MA, Gupta K, Hasselmo ME. 2011. Reduction of theta rhythm dissociates grid cell spatial periodicity from directional tuning. *Science* 332:595–599.
- Brandon MP, Bogaard AR, Schultheiss NW, Hasselmo ME. 2013. Segregation of cortical head direction cell assemblies on alternating θ cycles. *Nat Neurosci* 16:739–748.
- Brandon MP, Koenig J, Leutgeb JK, Leutgeb S. 2014. New and distinct hippocampal place codes are generated in a new environment during septal inactivation. *Neuron* 82:789–796.
- Burgess N. 2008. Grid cells and theta as oscillatory interference: Theory and predictions. *Hippocampus* 18:1157–1174.
- Burgess N, Recce M, O'Keefe J. 1994. A model of hippocampal function. *Neural Networks* 7:1065–1081.
- Bush D, Burgess N. 2014. A hybrid oscillatory interference/continuous attractor network model of grid cell firing. *J Neurosci* 34:5065–5079.
- Buzsáki G. 2002. Theta oscillations in the hippocampus. *Neuron* 33:325–340.
- Buzsáki G, Anastassiou CA, Koch C. 2012. The origin of extracellular fields and currents—EEG, ECoG, LFP and spikes. *Nat Rev Neurosci* 13:407–420.
- Buzsáki G, Leung LW, Vanderwolf CH. 1983. Cellular bases of hippocampal EEG in the behaving rat. *Brain Res* 287:139–171.

- Cacucci F, Lever C, Wills TJ, Burgess N, O'Keefe J. 2004. Theta-modulated place-by-direction cells in the hippocampal formation in the rat. *J Neurosci* 24:8265–8277.
- Chen SS. 2014. Another particle swarm toolbox. (<http://www.mathworks.com/matlabcentral/fileexchange/25986>), MATLAB Central File Exchange. Retrieved August 7, 2014.
- Climer JR, Newman EL, Hasselmo ME. 2013. Phase coding by grid cells in unconstrained environments: Two-dimensional phase precession. *Eur J Neurosci* 38:2526–2541.
- Colgin LL. 2013. Mechanisms and functions of theta rhythms. *Annu Rev Neurosci* 36:295–312.
- Colgin LL, Denninger T, Fyhn M, Hafting T, Bonnevie T, Jensen O, Moser MB, Moser EI. 2009. Frequency of gamma oscillations routes flow of information in the hippocampus. *Nature* 462:353–357.
- Csicsvari J, Hirase H, Czurko A, Mamiya A, Buzsáki G. 1999. Oscillatory coupling of hippocampal pyramidal cells and interneurons in the behaving Rat. *J Neurosci* 19:274–287.
- Davidson TJ, Kloosterman F, Wilson MA. 2009. Hippocampal replay of extended experience. *Neuron* 63:497–507.
- Deshmukh SS, Yoganarasimha D, Voicu H, Knierim JJ. 2010. Theta modulation in the medial and the lateral entorhinal cortices. *J Neurophysiol* 104:994–1006.
- Domnisoru C, Kinkhabwala AA, Tank DW. 2013. Membrane potential dynamics of grid cells. *Nature* 1–6.
- Dragoi G, Carpi D, Recce ML, Csicsvari J, Buzsáki G. 1999. Interactions between hippocampus and medial septum during sharp waves and theta oscillation in the behaving rat. *J Neurosci* 19:6191–6199.
- Eberhard RC, Shi Y, Kennedy J. 2001. *Swarm Intelligence*. San Diego, CA: Academic Press.
- Erchova I, Kreck G, Heinemann U, Herz AVM. 2004. Dynamics of rat entorhinal cortex layer II and III cells: Characteristics of membrane potential resonance at rest predict oscillation properties near threshold. *J Physiol* 560:89–110.
- Ermentrout GB, Galán RF, Urban NN. 2008. Reliability, synchrony and noise. *Trends Neurosci* 31:428–434.
- Fenton AA, Muller RU. 1998. Place cell discharge is extremely variable during individual passes of the rat through the firing field. *Proc Natl Acad Sci USA* 95:3182–3187.
- Fox SE, Wolfson S, Ranck JB. 1986. Hippocampal theta rhythm and the firing of neurons in walking and urethane anesthetized rats. *Exp Brain Res* 62:495–508.
- Fyhn M, Molden S, Witter MP, Moser EI, Moser MB. 2004. Spatial representation in the entorhinal cortex. *Science* 305:1258–1264.
- Green JD, Arduini AA. 1954. Hippocampal electrical activity in arousal. *J Neurophysiol* 17:533–557.
- Gutkin BS, Ermentrout GB, Reyes AD. 2005. Phase-response curves give the responses of neurons to transient inputs. *J Neurophysiol* 94:1623–1635.
- Hafting T, Fyhn M, Molden S, Moser MB, Moser EI. 2005. Microstructure of a spatial map in the entorhinal cortex. *Nature* 436:801–806.
- Hafting T, Fyhn M, Bonnevie T, Moser MB, Moser EI. 2008. Hippocampus-independent phase precession in entorhinal grid cells. *Nature* 453:1248–1252.
- Hahn TTG, McFarland JM, Berberich S, Sakmann B, Mehta MR. 2012. Spontaneous persistent activity in entorhinal cortex modulates cortico-hippocampal interaction in vivo. *Nat Neurosci* 15:1531–1538.
- Hasselmo ME. 2005. What is the function of hippocampal theta rhythm?—Linking behavioral data to phasic properties of field potential and unit recording data. *Hippocampus* 15:936–949.
- Heys JG, Giocomo LM, Hasselmo ME. 2010. Cholinergic modulation of the resonance properties of stellate cells in layer II of medial entorhinal cortex. *J Neurophysiol* 104:258–270.
- Heys JG, MacLeod KM, Moss CF, Hasselmo ME. 2013. Bat and rat neurons differ in theta-frequency resonance despite similar coding of space. *Science* 340:363–367.
- Hölscher C, Anwyl R, Rowan MJ. 1997. Stimulation on the positive phase of hippocampal theta rhythm induces long-term potentiation that can be depotentiated by stimulation on the negative phase in area CA1 in vivo. *J Neurosci* 17:6470–6477.
- Hutcheon B, Yarom Y. 2000. Resonance, oscillation and the intrinsic frequency preferences of neurons. *Trends Neurosci* 23:216–222.
- Huxter JR, Senior TJ, Allen K, Csicsvari J. 2008. Theta phase-specific codes for two-dimensional position, trajectory and heading in the hippocampus. *Nat Neurosci* 11:587–594.
- Hyman JM, Wyble BP, Goyal V, Rossi CA, Hasselmo ME. 2003. Stimulation in hippocampal region CA1 in behaving rats yields long-term potentiation when delivered to the peak of theta and long-term depression when delivered to the trough. *J Neurosci* 23:11725–11731.
- Jeewajee A, Barry C, O'Keefe J, Burgess N. 2008. Grid cells and theta as oscillatory interference: Electrophysiological data from freely moving rats. *Hippocampus* 18:1175–1185.
- King C, Recce M, O'Keefe J. 1998. The rhythmicity of cells of the medial septum/diagonal band of Broca in the awake freely moving rat: Relationships with behaviour and hippocampal theta. *Eur J Neurosci* 10:464–477.
- Koenig J, Linder AN, Leutgeb JK, Leutgeb S. 2011. The spatial periodicity of grid cells is not sustained during reduced theta oscillations. *Science* 332:592–595.
- Long LL, Hinman JR, Chen C-M, Escabi MA, Chrobak JJ. 2014. Theta dynamics in rat: Speed and acceleration across the septotemporal axis. *PLoS One* 9:e97987.
- Macadar O, Roig JA, Monti JM, Budelli R. 1970. The functional relationship between septal and hippocampal unit activity and hippocampal theta rhythm. *Physiol Behav* 5:1443–1449.
- Mattia M, Sanchez-Vives MV. 2012. Exploring the spectrum of dynamical regimes and timescales in spontaneous cortical activity. *Cogn Neurodyn* 6:239–250.
- Newman EL, Gillet SN, Climer JR, Hasselmo ME. 2013. Cholinergic blockade reduces theta-gamma phase amplitude coupling and speed modulation of theta frequency consistent with behavioral effects on encoding. *J Neurosci* 33:19635–19646.
- Newman EL, Climer JR, Hasselmo ME. 2014. Grid cell spatial tuning reduced following systemic muscarinic receptor blockade. *Hippocampus* 24:643–655. doi: 10.1002/hipo.22253.
- O'Keefe J, Burgess N. 2005. Dual phase and rate coding in hippocampal place cells: Theoretical significance and relationship to entorhinal grid cells. *Hippocampus* 15:853–866.
- O'Keefe J, Recce ML. 1993. Phase relationship between hippocampal place units and the EEG theta rhythm. *Hippocampus* 3:317–330.
- Park J, Lee H, Kim T, Park G, Lee E, Baek S, Kim I, Kim S, Jang DP, Kang J. 2014. Role of low- and high-frequency oscillations in the human hippocampus for encoding environmental novelty during a spatial navigation task. *Hippocampus* 24:1–12.
- Ray S, Naumann R, Burgalossi A, Tang Q, Schmidt H, Brecht M. 2014. Grid-layout and theta-modulation of layer 2 pyramidal neurons in medial entorhinal cortex. *Science* 343:891–896.
- Remme MW, Lengyel M, Gutkin BS. 2010. Democracy-independence trade-off in oscillating dendrites and its implications for grid cells. *Neuron* 66:429–437.
- Richard GR, Titiz A, Tyler A, Holmes GL, Scott RC, Lenck-Santini P-P. 2013. Speed modulation of hippocampal theta frequency correlates with spatial memory performance. *Hippocampus* 23:1269–1279.
- Sambeth A, Meeter M, Blokland A. 2009. Hippocampal theta frequency and novelty. *Hippocampus* 19:407–408; author reply 409–410.

- Sanchez-Vives MV, McCormick DA. 2000. Cellular and network mechanisms of rhythmic recurrent activity in neocortex. *Nat Neurosci* 3:1027–1034.
- Sanchez-vives MV, Mattia M, Compte A, Perez-Zabalza M, Winograd M, Descalzo VF, Reig R. 2010. Inhibitory Modulation of Cortical Up States. *J Neurophysiol* 104:1314–1324.
- Schmidt-Hieber C, Häusser M. 2013. Cellular mechanisms of spatial navigation in the medial entorhinal cortex. *Nat Neurosci* 16:325–331.
- Skaggs WE, McNaughton BL, Wilson MA, Barnes CA. 1996. Theta phase precession in hippocampal neuronal populations and the compression of temporal sequences. *Hippocampus* 6:149–172.
- Spaak E, Zeitler M, Gielen S. 2012. Hippocampal theta modulation of neocortical spike times and gamma rhythm: A biophysical model study. *PLoS One* 7:e45688.
- Stewart M, Fox SE. 1991. Hippocampal theta activity in monkeys. *Brain Res* 538:59–63.
- Tesche CD, Karhu J. 2000. Theta oscillations index human hippocampal activation during a working memory task. *Proc Natl Acad Sci USA* 97:919–924.
- Uhlhaas PJ, Pipa G, Lima B, Melloni L, Neuenschwander S, Nikolic D, Lin S. 2009. Neural synchrony in cortical networks: History, concept and current status. *Front Integr Neurosci* 3:1–19.
- Vanderwolf CH. 1969. Hippocampal electrical activity and voluntary movement in the rat. *Electroencephalogr Clin Neurophysiol* 26:407–418.
- Vinogradova OS, Brazhnik ES, Karanov AM, Zhadina SD. 1980. Neuronal activity of the septum following various types of deafferentation. *Brain Res* 187:353–368.
- Watrous AJ, Fried I, Ekstrom AD. 2011. Behavioral correlates of human hippocampal delta and theta oscillations during navigation. *J Neurophysiol* 105:1747–1755.
- Yartsev MM, Ulanovsky N. 2013. Representation of three-dimensional space in the hippocampus of flying bats. *Science* 340:367–372.
- Yartsev MM, Witter MP, Ulanovsky N. 2011. Grid cells without theta oscillations in the entorhinal cortex of bats. *Nature* 479:103–107.
- Yartsev MM, Witter MP, Ulanovsky N. 2012. Yartsev et al. reply to Barry OC, Bush D, O’Keefe J, Burgess N. *Nature* 488:E2–3.
- Zhou P, Burton SD, Urban NN, Ermentrout GB. 2013. Impact of neuronal heterogeneity on correlated colored noise-induced synchronization. *Front Comput Neurosci* 7:113.
- Zilli EA. 2012. Models of grid cell spatial firing published 2005–2011. *Front Neural Circuits* 6:16.
- Zilli EA, Yoshida M, Tahvildari B, Giocomo LM, Hasselmo ME. 2009. Evaluation of the oscillatory interference model of grid cell firing through analysis and measured period variance of some biological oscillators. *PLoS Comput Biol* 5:e1000573.